

Independent Contact Regions Based on a Patch Contact Model

Krzysztof Charusta, Robert Krug, Dimitar Dimitrov, and Boyko Iliev
Center of Applied Autonomous Sensor Systems (AASS), Örebro University, Sweden
Email: {krzysztof.charusta, robert.krug, dimitar.dimitrov, boyko.iliev}@oru.se

Abstract—The synthesis of multi-fingered grasps on non-trivial objects requires a realistic representation of the contact between the fingers of a robotic hand and an object. In this work, we use a patch contact model to approximate the contact between a rigid object and a deformable anthropomorphic finger. This contact model is utilized in the computation of Independent Contact Regions (ICRs) that have been proposed as a way to compensate for shortcomings in the finger positioning accuracy of robotic grasping devices. We extend the ICR algorithm to account for the patch contact model and show the benefits of this solution.

I. INTRODUCTION

Dexterous robotic hands have often been considered as the most natural choice for robotic applications that require grasping and manipulation of complex objects in unstructured environments. Multi-fingered anthropomorphic hands are especially suitable for manipulation of objects, such as tools and household objects, whose size and shape are designed to match the capabilities of the human hand. However, the large number of degrees of freedom in robotic hands and the complex sensing and actuation schemes make it rather difficult to apply traditional methods for grasp planning and control. An attractive alternative to analytical grasp synthesis methods is provided by the concept of human demonstration. Humans are able to provide practically an unlimited number of grasp examples with desired properties on arbitrary objects. Moreover, these grasps naturally incorporate task specific constraints, and anthropomorphic robotic hands are designed to replicate such grasps. In this line of research, Aleotti et al. [1] presented a method for interactive teaching of robotic grasps. Their approach considers a given grasp quality criterion and utilizes the established point contact model [2] to describe the interaction between object and fingers.

Analytical approaches for grasp synthesis usually rely on perfect knowledge of the object geometry. The consequence is that generated grasps guarantee the satisfaction of a desired quality criterion only if the robot hand grasps the object exactly at the prescribed contact points. Since this is hard to achieve in real world applications, an equally important property of a grasp is its robustness to positioning and synthesis inaccuracies. In this context, the notion of independent contact regions was proposed by Nguyen [3]. He defined the set of optimal independent regions with the largest minimal radius that yield a force-closure grasp if each finger is placed anywhere within its respective region. The concept was extended to the computation of independent regions for three-fingered grasps on planar objects [4] and

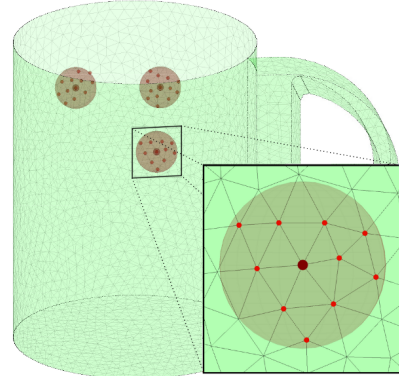


Fig. 1. A three-fingered grasp with a patch contact. Contact points forming the grasp are marked using red dots. The center points of patches are depicted using bigger dots.

four-fingered grasps on polyhedral objects by Ponce et al. [5]. In [6], Pollard employs the concept of ICRs to synthesize *grasp families* from a single demonstration of a whole-hand grasp targeted at cases where a large number of contacts is needed. Roa et al. [7] and later Krug et al. [8] present approaches for the computation of ICRs of precision grasps, which are represented as sets of single contact points.

In this article, we propose an approach to grasp synthesis that combines the intuitiveness of the human demonstration paradigm with the robustness provided by the concept of independent contact regions. The execution of precision grasps as demonstrated by a human using an anthropomorphic robotic gripper requires the solution of several problems, two of which we address in this paper. First, human demonstrations are inherently inaccurate due to the limited capabilities of the systems used to record the demonstration. These types of uncertainty can be dealt with by employing the concept of ICR. The second problem is that the contact between a deformable finger and an object is not limited to a single point but rather to a contact area. Hence, the representation of a human precision grasp by a point contact model might not be adequate in many cases, for example when grasping an object on a sharp edge or on the a handle of a cup. Note that a human grasp demonstration has (to some degree) an underlying assumption of a multi-point contact. The intended properties of a demonstrated grasp can be lost when a crude approximation as the single-point contact is used. Hence, analysis (*e.g.*, in the context of ICR) of human demonstrations based on a single point contact could be misleading.

For these reasons, we use a representation of a precision

grasp that is not defined as a set of single contact points. Instead, each contact between a finger and the object is represented as a *patch* that comprises a set of point contacts and accounts for the fact that a deformable finger can adapt to the surface of the grasped object (see Fig. 1). The main contribution of this article is the extension of the ICR algorithm [8] to precision grasps modeled by patches on the surface of an object. We show that this extension results in grasp families that better capture the properties of a grasp obtained from a human demonstration, which "by design" relies on a surface contact.

This article is organized as follows: Section II provides background before the concept of the patch contact model is introduced in Section III. Subsequently, a generalized version of the ICR algorithm is described in Section IV. We evaluate in simulation the proposed algorithm in Section V and draw conclusions in Section VI.

II. BACKGROUND

A. Nomenclature

- F - number of fingers in a grasp.
- S - number of points on the object surface.
- L - discretization of a friction cone.
- $f \in \{1 \dots F\}$ – index used for fingers.
- $s, z \in \{1 \dots S\}$ – indices used for contact points.
- $l \in \{1 \dots L\}$ – index used for forces and wrenches in a contact model.
- \mathbf{p}_s – a point on the surface of the object.
- \mathcal{O} - set containing the indices of all points on the discretized surface of the object $\mathcal{O} = \{1, \dots, S\}$.
- \mathcal{G} - a grasp – set of indices of points on the object surface in contact with all fingers, $\mathcal{G} \subset \mathcal{O}$.

B. Assumptions & Problem Description

The surface of an object is given as a discretized polygonal mesh of points and represented as a set $\{\mathbf{p}_s \in \mathbb{R}^3 : s \in \mathcal{O}\}$ with corresponding inward-pointing unit normals \mathbf{n}_s . The mesh is assumed to be sufficiently discretized to capture the local curvature of an object. Each point \mathbf{p}_s has a neighborhood $\mathcal{N}(s)$ defined as a set of indices of those points which are connected to \mathbf{p}_s by an edge of the polygonal mesh. Furthermore, we assume that a user-input is available in form of an initial grasp. It can be acquired either by a human demonstration or by one of the many algorithms proposed for grasp synthesis (*e.g.*, [7][9]). We will use \mathcal{I} to denote the set containing indices of points on the object surface that are the centers of the initial contact patches.

$$\mathcal{I} = \{s : s \in \mathcal{O}\}, |\mathcal{I}| = F. \quad (1)$$

Each $\{\mathbf{p}_s : s \in \mathcal{I}\}$ is a point on the discrete surface of an object, where the center of a contact patch between the robotic finger and the object is located. For example, $\mathcal{I} = \{11, 113, 531\}$ means that the centers of three contact patches are at locations \mathbf{p}_{11} , \mathbf{p}_{113} and \mathbf{p}_{531} .

C. Forces and Friction

One key aspect of modeling a grasp is the definition of a contact model between the surface of the object to be grasped and the fingers of a gripper. We adopt Coulomb's friction model, which states that slippage between two contacting surfaces does not occur if the following condition is satisfied

$$\|(\mathbf{I} - \mathbf{n}_s \mathbf{n}_s^T) \mathbf{f}_s\|_2 \leq \mu (\mathbf{n}_s^T \mathbf{f}_s), \quad (2)$$

where \mathbf{f}_s is the contact force, $\mu \in \mathbb{R}_+$ is a friction coefficient, and \mathbf{I} is the identity matrix (with appropriate dimensions).

The nonlinear inequality (2) is commonly approximated by an L -sided polyhedral cone. The forces along the L edges of the discretized cone with its apex at contact point \mathbf{p}_s are denoted in matrix notation as

$$\mathbf{F}_s = [\mathbf{f}_1(s) \quad \dots \quad \mathbf{f}_L(s)].$$

A contact force \mathbf{f}_s can be expressed as a conic combination of forces \mathbf{F}_s , or formally

$$\mathbf{f}_s = \mathbf{F}_s \boldsymbol{\alpha}_s, \quad \boldsymbol{\alpha}_s \geq \mathbf{0}. \quad (3)$$

The force \mathbf{f}_s creates a torque $\boldsymbol{\tau}_s = (\mathbf{p}_s \times \mathbf{f}_s)$ about the origin of the reference frame. Force and torque vectors can be concatenated to form a wrench

$$\mathbf{w}_s = \begin{pmatrix} \mathbf{f}_s \\ \boldsymbol{\tau}_s / \lambda \end{pmatrix}, \quad \lambda = \max_s (\|\mathbf{p}_s\|_2). \quad (4)$$

Dividing the torque part of \mathbf{w}_s by the largest torque arm λ guarantees scale invariance [10]. The wrenches generated by forces \mathbf{f}_l along the edges of the discretized friction cone are referred to as *primitive wrenches*. For a given contact point \mathbf{p}_s , the set of primitive wrenches

$$\mathcal{W}[s] = \{\mathbf{w}_1(s), \dots, \mathbf{w}_L(s)\} \quad (5)$$

forms a cone in the wrench space.

In a similar fashion we denote a set of wrenches associated to more than one contact point, *e.g.*, all wrenches associated with the contact points of grasp \mathcal{G} are denoted by $\mathcal{W}[\mathcal{G}]$.

D. Wrench spaces

Suppose we are given a grasp \mathcal{G} , the set of all wrenches that can be applied to an object through this grasp (assuming bounded contact forces) is called the *Grasp Wrench Space* (GWS). Formally, the GWS is defined as the convex hull of the primitive wrenches associated to the contact points in \mathcal{G}

$$\text{GWS} = \text{ConvexHull}(\mathcal{W}[\mathcal{G}]). \quad (6)$$

Note that not necessarily all wrenches in $\mathcal{W}[\mathcal{G}]$ are vertices of the GWS (*e.g.*, when the grasp \mathcal{G} contains multiple points on a planar surface, some of this wrenches may lie on ridges of the GWS).

The *Object Wrench Space* (OWS) is the union of the grasp wrench spaces of all possible grasps for a given object. Formally, the OWS is defined as the convex hull of the primitive wrenches associated to all points of the mesh describing the geometry of an object.

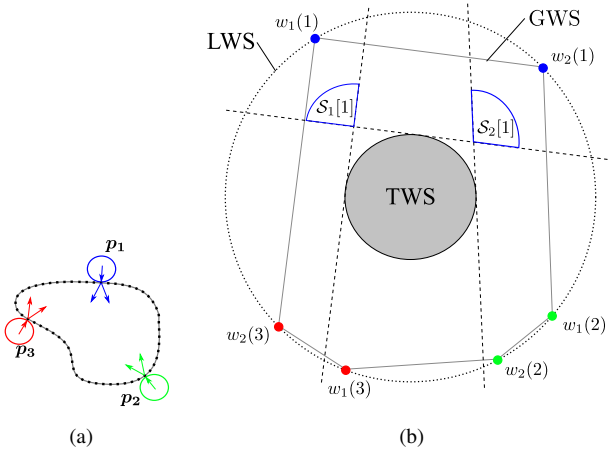


Fig. 2. (a) A three-fingered grasp on a discretized planar object. All contacts are described by the single-point contact model, $\mathcal{G} = \mathcal{I} = \{1, 2, 3\}$. (b) Abstract 2-dimensional representation of the resulting GWS and the chosen TWS; Also shown are the two search zones $\mathcal{S}_1[1]$ and $\mathcal{S}_2[1]$ corresponding to \mathbf{p}_1 (see Section IV-A).

The *Limit Wrench Space* (LWS) [10] is the union of the object wrench spaces of all possible objects. It is bounded by the convex hull of all wrenches, which meet the general force and torques constraints – we assume that $\|\mathbf{f}_s\|_2 = 1$ and hence $\|\boldsymbol{\tau}_s\| \leq \lambda$ for all s . The OWS is a subset of the LWS.

Equation (6) characterizes the set of wrenches that can be exerted on the grasped object when the magnitudes of all applied forces sum up to a given bound. The geometry of the GWS is limited by the LWS and determined by the choice of finger positions on the object and has to fulfill requirements related to a given task.

A task is represented as a set of wrenches called the *Task Wrench Space* (TWS). It represents the set of wrenches that every viable grasp has to be able to exert on the object in order to counterbalance the disturbance wrenches acting on the object. Often the TWS is represented as an origin-centered ball (this relates to the grasp quality measure proposed in [11]). A grasp is said to be force-closure, if its GWS contains a neighborhood of the origin. If the TWS is contained in the GWS, then the task requirements are also fulfilled. Formally, the GWS, OWS, LWS, and TWS are not vector spaces. Nevertheless, we use this naming convention as it is commonly accepted in the literature.

Fig. 2 depicts GWS, TWS, and LWS of an example grasp that utilizes the single-point frictional contact model ($\mathcal{G} = \mathcal{I} = \{1, 2, 3\}$). A point $\mathbf{p}_{\mathcal{I}_f}$ has an associated wrench cone generated by the two primitive wrenches $\mathbf{w}_1(\mathcal{I}_f)$ and $\mathbf{w}_2(\mathcal{I}_f)$. For simplicity, a hypothetical 2-dimensional illustration of wrenches is adopted, although they are 6-dimensional in the general case and 3-dimensional for planar grasps.

III. THE PATCH CONTACT MODEL

A. Motivation

The single-point contact model has been widely used in robotic applications related to grasping [12] [6] [7] [8]. However, in scenarios where anthropomorphic robot hands with soft or deformable fingers are used, the single-point

contact model might not be realistic because it contains information only about wrenches that can be exerted through one single point. Usually, the contact surface of a soft finger is a patch. Thus, a more realistic contact model should contain information about wrenches that can be exerted through the entire contact area. As we will discuss in the following sections, such additional wrenches increase the volume of the GWS, making the contact model more realistic.

To model a deformable finger more accurately, Goyal et al. [13] introduced the notion of a *limit surface*, which later has been approximated by Howe et al. [14]. Given a planar contact between two bodies, the limit surface bounds the space of frictional forces and moments that the contact can resist without slipping. Ciocarlie et al. [15] use a planar contact patch on the object surface in their grasp analyses. The wrenches building the GWS are generated by forces along the discretized boundary of the patch, thus resulting in a larger volume of the GWS. In the remainder of this section we define a patch contact model similar to the one used in [15]. The patch approximates the contact between a deformable finger and the object surface and is used in Section IV to extend the ICR computation algorithm.

B. The Patch Contact

Let us assume that a fingertip has the shape of a ball made of elastic material. When in contact with a planar surface of a rigid object, the fingertip forms a circular contact. The radius of the contact is proportional to the normal force, and depends on the size, curvature, and material properties of the fingertip [16]. Motivated by the above assumptions, we define a patch centered at point \mathbf{p}_s as a set of point indices

$$\mathcal{P}(s, r) = \{z: \delta_s^z \leq r, z \in \mathcal{O}\}, \quad (7)$$

where $r \geq 0$ is a parameter that bounds the size of a patch, and δ_s^z is the shortest path along the edges of the polygonal mesh between points with indices s and z . In other words, a point with index z qualifies to be a member of a patch around \mathbf{p}_s if the distance from \mathbf{p}_s to \mathbf{p}_z (along the edges of the polygonal mesh) is less than or equal to r . Since the neighborhood $\mathcal{N}(s)$ of every point in the mesh is known, the patch $\mathcal{P}(s, r)$ can be computed using a simple breadth-first search with \mathbf{p}_s representing the root node.

The definition of a patch in (7) is not an attempt for precise physical modeling, as in [15]. It is rather a simple way of bounding the shape and area of contact of a deformable fingertip. Note that the patch always conforms to the shape of an object, hence the number and the distribution of points in a patch do not depend only on factors related to the finger, but also on the local curvature and the discretization of a mesh.

The proposed definition of a patch is flexible and could be used to represent a variety of finger contacts. As a special case, when the radius of a patch is equal to zero, it models a single-point contact. In such a case, the patch consists of only one contact point, thus $\mathcal{P}(s, 0) = \{s\}$. The definition could be extended to describe other contact geometries (*e.g.*, ellipsoidal) with different sizes for each finger. Nevertheless,

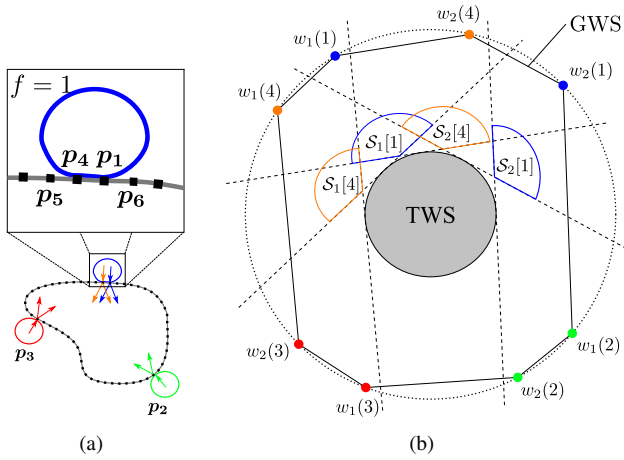


Fig. 3. (a) The same object as in Fig. 2 closed in a three-fingered precision grasp $\mathcal{G} = \{1, 2, 3, 4\}$. The contact of one of the fingers ($f = 1$) is represented as a patch containing two points $\mathcal{P}(1) = \{1, 4\}$. (b) Abstract 2-dimensional representation of the GWS associated to the grasp. Marked are the search zones associated to the patch $\mathcal{P}(1)$ (see Section IV-A).

for simplicity of notation, we limit the discussion to patches bounded by spheres with radius r , the same for all fingers. Hence, in the sequel the parameter r will be dropped for simplicity of notation.

In this paper the pressure distribution in a patch is not considered. The underlying assumption is that the resultant force exerted by a finger can lie anywhere within its respective patch.

C. The Grasp

Given the description of a patch in (7), we define an F -fingered grasp \mathcal{G} as a set of point indices participating in the patches that are centered at points with indices in \mathcal{I} , or formally

$$\mathcal{G} = \{s: s \in \mathcal{P}(\mathcal{I}_f), f = 1, \dots, F\}. \quad (8)$$

Note that the f^{th} patch in \mathcal{G} is centered at point $\mathcal{P}_{\mathcal{I}_f}$. An example of a grasp \mathcal{G} formed as a set of patches is depicted in Fig. 1.

As a consequence of using the patch contact model, if $r > 0$, the number of contact points participating in a grasp \mathcal{G} increases in comparison to grasps utilizing the single-point contact model, where $|\mathcal{G}| = F$. Thus, the number of wrenches forming the GWS of \mathcal{G} is also larger. Fig. 3 depicts essentially the same grasp as shown in Fig. 2, however, with the difference that one of the fingers utilizes a patch contact model. Fig. 3(b) depicts the GWS of this grasp. In this example, there are 4 primitive wrenches associated to the patch, namely $w_1(1)$, $w_2(1)$, $w_1(4)$, and $w_2(4)$ opposed to only $w_1(1)$ and $w_2(1)$ in case of the single-point contact model, as shown in Fig. 2(b).

Fig. 4 compares grasp wrench spaces associated with the two grasps from Fig. 2(a) and Fig. 3(a). The $\text{GWS}_{\mathcal{I}}$ corresponds to the grasp that employs the point contact model to all fingers, $\mathcal{G} = \mathcal{I}$. The GWS corresponds to a grasp comprising one patch contact in this example. Using the patch contact model increases the volume of the corresponding grasp wrench space due to additional wrenches

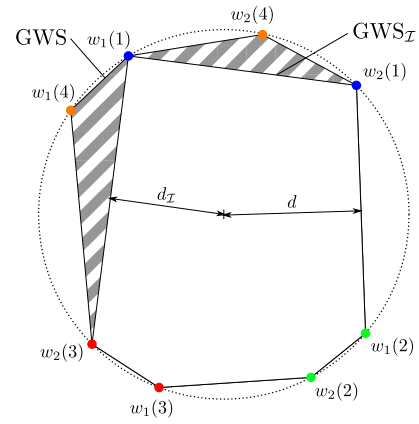


Fig. 4. Comparison of grasp wrench spaces: $\text{GWS}_{\mathcal{I}}$ of a grasp employing only the point contact model, and the GWS of a grasp with one patch contact. The volume difference is indicated by the dashed area. The maximal radii of respective origin-centered in-spheres are given by $d_{\mathcal{I}}$ and d .

contributed by the patch. In general, the GWS of any grasp formed using patches is a superset of the $\text{GWS}_{\mathcal{I}}$ of a grasp formed using the center points only. Also, considering the spherical quality metric proposed in [11], the radius of the largest origin-centered sphere possible to fit in the GWS is usually larger when employing patch contacts.

IV. THE PATCH-ICR

For a given F -fingered grasp, the ICR paradigm forms F regions as sets of discrete points on the object surface. Each of these regions corresponds to one finger of a grasping device. By construction, if each finger is placed inside its respective region, any resulting grasp is guaranteed to resist the predefined disturbances. According to Pollard [10], the set of these grasps constitutes a family of similar grasps. As assumed in Section II, the mesh is sufficiently discretized, thus an ICR can be considered as an area rather than a discrete region, *i.e.*, a grasp preserves the task even when a fingertip is located on one of the facets of a mesh that is spanned by points forming an ICR.

To our knowledge, the concept of ICR has only been used with the single-point contact model [6] [8] [10]. More elaborate models, as the one proposed in Section III, have not been considered yet. In this section, we introduce a generalization of the ICR concept that accounts for the patch contact model – the Patch-ICR ($\text{ICR}^{\mathcal{P}}$). In the following we give an explanation of how to construct $\text{ICR}^{\mathcal{P}}$ from the input grasp \mathcal{G} and then formalize the construction procedure into an algorithm.

A. Construction Procedure

The procedure of constructing $\text{ICR}^{\mathcal{P}}$ requires the following user input:

- definition of a task expressed as a TWS,
- a prototype grasp parametrized as a set of indices of initial center-points \mathcal{I} ,
- definitions of patches $\{\mathcal{P}(\mathcal{I}_f, r), f = 1 \dots F\}$.

In preliminary steps, a grasp \mathcal{G} is formed according to (8) and its GWS is calculated, which requires computation of the

convex hull in (6). If the task requirements are fulfilled, *i.e.*, the GWS contains the TWS (see Fig. 3(b)), the construction procedure of the ICRs ^{\mathcal{P}} can begin.

The GWS represents the set of all wrenches that the grasp \mathcal{G} can exerted on the object. During the preliminary step above we have verified that the TWS is a subset of the GWS. To this end, we can say that the grasp \mathcal{G} is redundant with respect to the task. This redundancy is directly related to the geometry of the GWS. Since we are only interested in being able to satisfy the task, we wish to trade-off this redundancy for the possibility to generate a family of grasps that is guaranteed to preserve the task requirements. This trade-off can be defined as an affine transformation of the GWS. Or, in other words, as a generation of a new polyhedron related to the GWS. The most commonly used way for performing this transformation is the procedure of inwards parallel shifting of the hyperplanes defining the GWS until they are tangent to the TWS [10]. An alternative approach (including altering the orientation of the hyperplanes) is discussed in [17]. Fig. 3(b) depicts conceptually the parallel shifting of some of the hyperplanes (shifted hyperplanes are depicted using dashed lines).

The process of transforming the GWS leads to the definition of zones in the wrench space that are used to identify a family of grasps, all of which satisfy the task. We associate a polyhedral *search zone* $\mathcal{S}_l[s]$ with each primitive wrench $w_l(s)$ that is a vertex of the GWS. This polyhedron is formed by the intersection of exterior half-spaces¹ defined by the hyperplanes that contained $w_l(s)$ before they underwent the affine transformation (*e.g.*, parallel shifting). We denote by \mathcal{S}^f the set of all search zones associated with the f^{th} finger centered at \mathcal{I}_f .

$$\mathcal{S}^f = \{\mathcal{S}_l[s] : \forall s \in \mathcal{P}(\mathcal{I}_f), \forall l_s\}, \quad (9)$$

where $\forall l_s$ in (9) stands for the indices of all wrenches (associated to a point with index s) that are vertices of the GWS.

Fig. 3(b) depicts the enlarged first finger ($f = 1$) that forms a patch contact. Both points with the index in patch $\mathcal{P}(1) = \{1, 4\}$ have two corresponding wrenches that are vertices of the GWS. Thus, there are four search zones associated with finger $f = 1$, namely

$$\mathcal{S}^1 = \{\mathcal{S}_1[1], \mathcal{S}_2[1], \mathcal{S}_1[4], \mathcal{S}_2[4]\}.$$

With reference to Fig. 3(b), note that any primitive wrench that is inside the search zone $\mathcal{S}_l[s]$ can substitute the wrench $w_l(s)$ in the GWS, thus resulting in a GWS that would still contain the TWS. A more formal discussion on the above statement can be found in [8], and a proof is given in [18]. The ability to find a substitute for a wrench inside its search zone is a key property underlying the construction of the independent contact regions.

¹A half-space is said to be exterior if it does not contain the origin, opposed to an interior half-space that contains the origin.

Definition 1 (ICR ^{\mathcal{P}}) Given a grasp \mathcal{G} and a task in form of a TWS, the f^{th} independent contact region (denoted by \mathcal{C}^f) associated with the patch $\mathcal{P}(\mathcal{I}_f)$ is defined as the set of indices $z \in \mathcal{O}$, each of which has the following properties:

- Each patch $\{\mathcal{P}(z) : z \in \mathcal{C}^f\}$ can substitute the original patch $\mathcal{P}(\mathcal{I}_f) \in \mathcal{G}$ without violating the task requirements.
- Each $z \in \mathcal{C}^f$ satisfies the inclusion conditions in Proposition 1.

The definition implies that each set \mathcal{C}^f contains the indices of points where the center of a patch corresponding to finger f can be placed.

Proposition 1 (Inclusion condition) The index $z \in \mathcal{O}$ is included in \mathcal{C}^f if for any search zone $\mathcal{S}_l[s] \in \mathcal{S}^f$ there exists an $s \in \mathcal{P}(z)$ such that any convex combination of elements of $\mathcal{W}[s]$ is in $\mathcal{S}_l[s]$.

Corollary 1 (Inclusion condition – simple) The index $z \in \mathcal{O}$ is included in \mathcal{C}^f if for any search zone $\mathcal{S}_l[s] \in \mathcal{S}^f$ there exists an $s \in \mathcal{P}(z)$ such that at least one element of $\mathcal{W}[s]$ is in $\mathcal{S}_l[s]$.

Proposition 1 follows from the geometric analysis carried out in [8]. Note that Proposition 1 supersedes Corollary 1 that is a more restrictive inclusion test but computationally less expensive. The results in Section V are generated using the inclusion condition according to Corollary 1.

The grasp family associated with \mathcal{G} is a set of F -fingered grasps that preserve predefined task requirements. To generate a grasp belonging to the family of \mathcal{G} we select F indices – one from each region $\{\mathcal{C}^f : f = 1 \dots F\}$, and form a set of patches centered at these indices using (7). A set of these patches forms a new member of the family, which we denote as

$$\mathcal{F}^{\mathcal{G}} = \{s : s \in \mathcal{P}(z_f), z_f \in \mathcal{C}^f, f = 1 \dots F\}. \quad (10)$$

Consider again Fig. 3(b) in context of the inclusion condition from Proposition 1. It depicts a three-fingered grasp $\mathcal{G} = \{1, 2, 3, 4\}$, where one of the fingers forms a patch involving points \mathbf{p}_1 and \mathbf{p}_4 (point \mathbf{p}_1 is assumed to be the center of the patch $\mathcal{P}(1) = \{1, 4\}$). In order to be able to form a new grasp in the family associated with \mathcal{G} we search for a patch that can substitute $\mathcal{P}(1)$ (and still preserves the chosen TWS). Possible candidates are patches centered at the neighbors $\mathcal{N}(1) = \{4, 6\}$ of \mathbf{p}_1 . Let us first consider $\mathcal{P}(6) = \{6, 1\}$ (\mathbf{p}_6 is assumed to be the center). Patch $\mathcal{P}(6)$ can substitute $\mathcal{P}(1)$ because wrenches $\mathcal{W}[1] = \{w_1(1), w_2(1)\}$ are located in all search zones \mathcal{S}^1 . Note that wrenches associated to \mathbf{p}_6 are not necessary to satisfy the task. In contrast, patch $\mathcal{P}(4) = \{4, 5\}$ (\mathbf{p}_4 is assumed to be the center) substitutes $\mathcal{P}(1)$ only if there exists a convex combination of wrenches $\mathcal{W}[5]$ (not depicted in the figure) in the search zone $\mathcal{S}_2[1]$ – which does not contain wrenches $\mathcal{W}[4] = \{w_1(4), w_2(4)\}$.

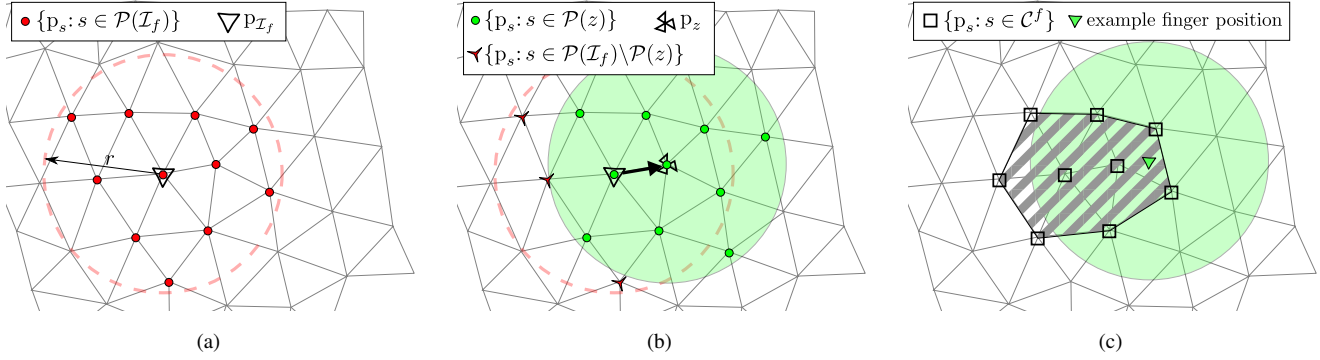


Fig. 5. Construction of a region \mathcal{C}^f . (a) Initial patch $\mathcal{P}(\mathcal{I}_f)$. (b) The first iteration of the algorithm. (c) \mathcal{C}^f generated after several iteration. The center of a patch, which represents a finger contact, can be placed anywhere inside the dashed area.

Algorithm 1 construction of $\text{ICRs}^{\mathcal{P}}$

- 1: **Input:** $r, \mathcal{I}, \{\mathcal{P}(\mathcal{I}_f)\}, \{\mathcal{S}^f\}, f \in 1 \dots F$
 - 2: **Variables:** $\hat{\mathcal{C}}$ = queue of candidate points; $\hat{\mathcal{V}}$ = indices of visited points; $\bar{\mathcal{S}}$ = empty search zones; Π = structure containing visited search zones
 - 3: **Output:** $\mathcal{C}^f, f = 1 \dots F$
 - 4: **for** $f = 1 \dots F$ **do**
 - 5: $\hat{\mathcal{C}} = \hat{\mathcal{V}} = \bar{\mathcal{S}} = \mathcal{C}^f = \emptyset$ {clear sets}
 - 6: $\hat{\mathcal{V}} = \mathcal{I}_f$ {classify \mathcal{I}_f as visited}
 - 7: $\hat{\mathcal{C}} = \mathcal{N}(\mathcal{I}_f)$ {initialize queue with neighbors of \mathcal{I}_f }
 - 8: **while** $\hat{\mathcal{C}} \neq \emptyset$ **do**
 - 9: $z \leftarrow \hat{\mathcal{C}}_1$ {dequeue the first element in $\hat{\mathcal{C}}$ }
 - 10: calculate $\mathcal{P}(z)$
 - 11: $\bar{\mathcal{S}} \leftarrow \mathcal{S}^f \setminus \Pi(\mathcal{P}(z))$ {select empty search zones}
 - 12: **if** $\text{InclusionTest}(\bar{\mathcal{S}}, \mathcal{W}[\mathcal{P}(z)]) = \text{true}$ **then**
 - 13: $\mathcal{C}^f \leftarrow z$ {qualify z as an $\text{ICR}^{\mathcal{P}}$ member}
 - 14: $\hat{\mathcal{C}} \leftarrow \mathcal{N}(z) \setminus \hat{\mathcal{V}}$ {enqueue unvisited neighbors}
 - 15: **end if**
 - 16: update Π
 - 17: $\bar{\mathcal{S}} = \emptyset$
 - 18: $\hat{\mathcal{V}} \leftarrow \hat{\mathcal{V}} \cup z$ {add z to the set of visited points}
 - 19: **end while**
 - 20: **end for**
-

B. Algorithm

Here, we analyze the key aspects of the construction procedure of $\text{ICRs}^{\mathcal{P}}$, which is summarized in Algorithm 1. It is assumed that the preliminary steps discussed in Section IV-A are completed, and for each finger $f \in \{1 \dots F\}$ search zones \mathcal{S}^f are computed – *e.g.*, by using the hyperplane parallel shifting approach [8]. Algorithm 1 is based on a breath-first search and can be conducted independently for each finger.

The algorithm starts with contact point index \mathcal{I}_f . First, neighbours $\mathcal{N}(\mathcal{I}_f)$ are added to the queue $\hat{\mathcal{C}}$, to then be tested one-by-one for inclusion in region \mathcal{C}^f . For each point index z dequeued from $\hat{\mathcal{C}}$, a patch $\mathcal{P}(z)$ is computed and its wrenches $\mathcal{W}[\mathcal{P}(z)]$ are used as an input to the inclusion test in Proposition 1. If the test succeeds, z is added to the region \mathcal{C}^f and the neighbors of z are enqueued in $\hat{\mathcal{C}}$. The algorithm terminates when $\hat{\mathcal{C}}$ is empty, *i.e.*, when there are no points

left to explore.

Since the algorithm utilizes a simple breath-first exploration scheme, frequently two overlapping patches share common points, thus common wrenches. Therefore, to increase the efficiency of the algorithm the results of the inclusion test are stored in a container Π . For each index $\{s: s \in \mathcal{P}(z), z \in \hat{\mathcal{V}}\}$, the container Π stores a set of search zones from \mathcal{S}^f that contain at least one wrench from the set $\mathcal{W}[s]$. We denote by $\Pi(s)$ a query that returns a set of search zones which, in previous iterations, have been verified to contain at least one wrench $w_i(s) \in \mathcal{W}_i[s]$. If s participates in a patch during subsequent iterations of the algorithm these search zones do not need to be checked again. In each iteration, a set of remaining empty search zones $\bar{\mathcal{S}} \subseteq \mathcal{S}^f$ is obtained as $\bar{\mathcal{S}} = \mathcal{S}^f \setminus \Pi(\mathcal{P}(z))$.

To give a better view on the construction of $\text{ICRs}^{\mathcal{P}}$ let us examine Fig. 5(a) depicting a patch $\mathcal{P}(\mathcal{I}_f)$ centered at initial point $p_{\mathcal{I}_f}$. In the first iteration of the algorithm (see Fig. 5(b)), a point p_z is being tested for inclusion. Having two partially overlapping patches ($\mathcal{P}(\mathcal{I}_f)$ and $\mathcal{P}(z)$), the information from structure Π is used to determine search zones that are already filled. Subsequently, in the inclusion test, it is checked if any wrench in $\mathcal{W}[\mathcal{P}(z)]$ fills the remaining empty search zones $\bar{\mathcal{S}}$. In Fig. 5(b), points associated to the empty zones are marked using red stars. The inclusion test terminates if either Proposition 1 is satisfied or there is no wrench in $\mathcal{W}[\mathcal{P}(z)]$ that satisfies it. After several iterations of the algorithm, the region \mathcal{C}^f is created (see Fig. 5(c)). The center of a patch can be safely placed anywhere inside the region (depicted as the dashed area) without violating the task.

The described algorithm for generating $\text{ICRs}^{\mathcal{P}}$ has been implemented in Matlab as a proof-of-concept without prioritizing computational efficiency. Nevertheless, we briefly discuss the computational complexity of the algorithm. The three most computationally expensive steps are the following. First, the construction of the GWS. In this step, a 6D convex hull over $L|\mathcal{G}|$ primitive wrenches is computed, where L is the friction cone discretization. Considering the QuickHull algorithm [19], this step has a complexity of $O((L|\mathcal{G}|)^3/6)$. Second, for each candidate point in the queue $\hat{\mathcal{C}}$, Algorithm 1 computes a patch. Since the neighborhood of each point p_s is

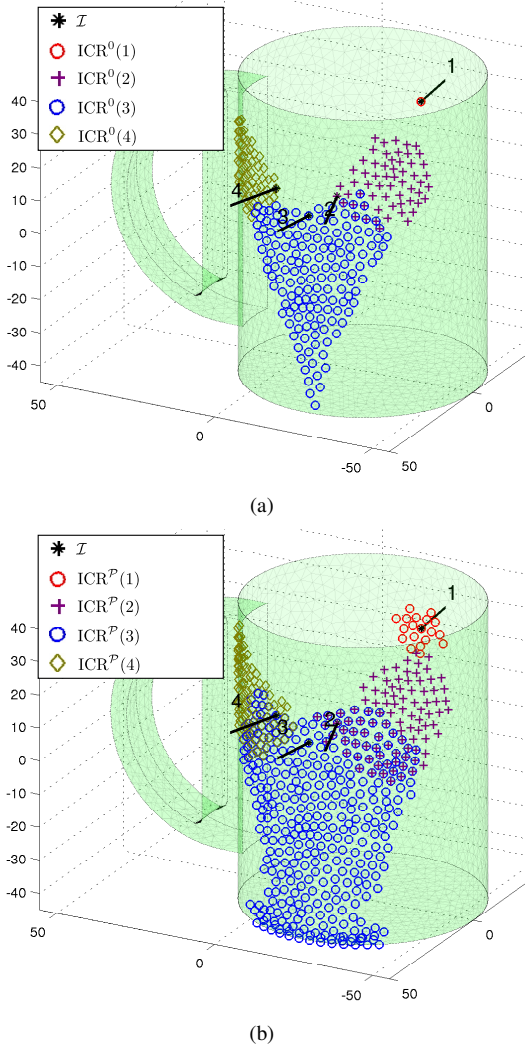


Fig. 6. The resulting $\text{ICRs}^{\mathcal{P}}$ according to Algorithm 1 for an anthropomorphic 4-fingered grasp with an opposing thumb ($\mu = 1$, $\alpha = 0.56$), contact model: (a) the single-point contact with friction. (b) the patch contact with friction, parameter $r = 6\text{mm}$.

known in advance, the complexity of forming a patch using (7) is $O(S + E)$, where E is the number of edges connecting vertices of the mesh. Finally, evaluating the inclusion test according to Proposition 1 requires the solution of a linear programming problem. Since the calculation of each region can be done independently, Algorithm 1 can be parallelized in the number of fingers participating in a grasp.

V. RESULTS

In this section we demonstrate the validity of the patch representation and the applicability of the presented algorithm for generating ICRs. We used two different contact models, the single-point contact model (with friction), and the patch contact model (with friction). We refer to the results obtained using the former as ICR^0 and to the results generated using the latter as $\text{ICR}^{\mathcal{P}}$. The center points \mathcal{I} were acquired in a human demonstration phase using a motion capturing setup [20]. The ICRs^0 were directly generated

from the grasp $\mathcal{G} = \mathcal{I}$ (*i.e.*, $r = 0$). To calculate $\text{ICR}^{\mathcal{P}}$ the grasp \mathcal{G} was obtained via (7) and (8). In the experiments, the TWS was represented as an origin-centered ball, the same for both contact models. In each experiment the radius was set as a fraction α of the largest origin-centered ball that fits into the respective $\text{GWS}_{\mathcal{I}}$. Search zones were formed using parallel shifting as in [8]. To show the benefits of $\text{ICRs}^{\mathcal{P}}$, the two different contact representations are compared on two objects. The geometric center of the object was used as an origin of the reference frame.

In the first experiment, an anthropomorphic 4-fingered grasp with an opposing thumb was demonstrated on a cup. Parameters $\alpha = 0.56$, and friction coefficient $\mu = 1$ were chosen. The ICRs computed on this object are depicted in Fig. 6. We observe in Fig. 6(a) that when the single-point contact model was used, $\text{ICR}^0(1)$ associated with the thumb contains only one contact point. It is evident that in this case the point contact model is not adequate, since it does not leave any space for finger misplacement. A patch (if it contains more than one point) contributes more primitive wrenches that span the GWS. In Fig. 6(b) patches parametrized by $r = 6\text{mm}$ for all fingers are used (friction coefficient and TWS are the same as in Fig. 6(a)). It is clearly visible that $\text{ICRs}^{\mathcal{P}}$ of all fingers are larger and more balanced, compared to the results obtained with the point contact model.

In the second experiment, we consider a scenario in which a human demonstrates a 3-fingered grasp on a pencil. When the point contact model is used, only three single-contact points are placed on the hexagonal shape of the pencil, as depicted in Fig. 7(a). ICRs^0 generated from this initial grasp do not represent the true grasping possibilities. Such an “unintuitive” output occurs because of two reasons: (i) the ICR algorithm is very sensitive to the initial placement of fingers when the single-point contact model is used; (ii) the single-point contact model does not exert as many primitive wrenches as the soft deformable finger in reality. In comparison, $\text{ICRs}^{\mathcal{P}}$ (depicted in Fig. 7(b)) were computed utilizing patches parametrized by $r = 3\text{mm}$. Again, the same TWS and $\mu = 1$ is used. The patch contact envelopes the geometry of the pencil. As a consequence, the generated $\text{ICRs}^{\mathcal{P}}$ are significantly larger and resembles a grasp family corresponding to a hand with deformable fingers in a more realistic fashion.

To give an idea about the execution time of the presented ICR algorithm, trial series of experiments were performed. Five anthropomorphic grasps on the model of a cup were generated. The execution time of the algorithm was measured for the patch parameter r ranging from 1mm to 10mm. The size of a patch directly relates to the number of contact points in a grasp \mathcal{G} , which has a major influence on the time performance. Fig. 8 presents the execution time as a function of $|\mathcal{G}|$. The time evaluation was performed on a Core2Duo 2 GHz computer.

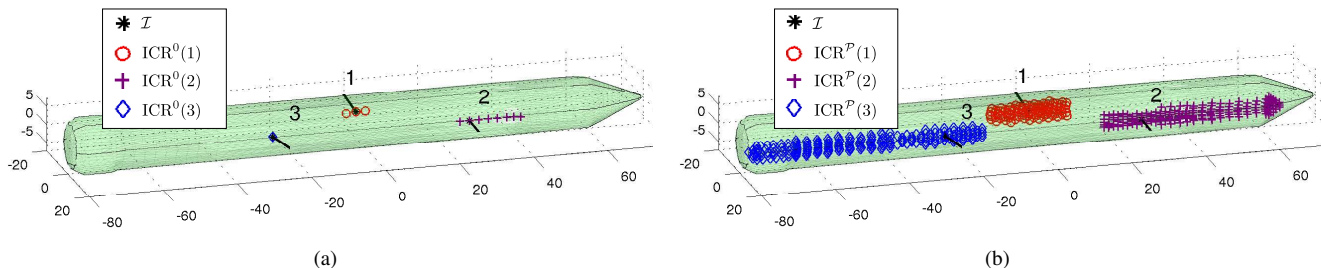


Fig. 7. ICRs generated with different contact models. Friction coefficient $\mu = 1$, parameter $\alpha = 0.56$ (a) the single-point contact model, (b) the patch contact, $r = 3\text{mm}$.

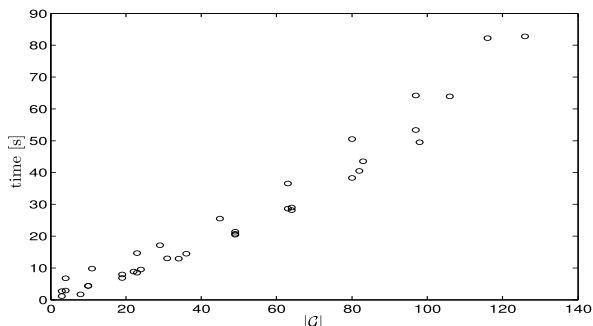


Fig. 8. The execution time of the ICR algorithm as function of grasp size $|G|$.

VI. SUMMARY

This paper presents an extension of the concept of Independent Contact Regions (ICRs). Instead of the commonly used single-point contact, we adopt a *patch* contact model that captures in a more realistic way the contact between a rigid object and a deformable finger. We show that the patch contact model used in the context of ICRs results in grasp families that better capture the properties of a grasp obtained from a human demonstration (which “by design” relies on a surface contact).

We propose a computation algorithm and evaluate our solution in simulation on models of two real objects, using grasps acquired via human demonstration. The benefits of using the patch contact model in the context of ICRs are especially apparent when considering grasps with contacts on edges.

More detailed research is needed to evaluate the reliability of the generated independent regions in real-world robot grasping applications. Further work on an efficient implementation is also necessary.

VII. ACKNOWLEDGMENTS

This research has been partially supported by the HAN-DLE project, funded by the European Community’s Seventh Framework Programme (FP7/2007-2013) under grant agreement ICT 231640.

REFERENCES

- [1] S. C. J. Aleotti, “Interactive teaching of task-oriented robot grasps,” *Robotics and Autonomous Systems*, vol. 58, no. 5, pp. 539–550, 2010.
- [2] R. M. Murray, S. S. Sastry, and L. Zexiang, *A Mathematical Introduction to Robotic Manipulation*, 1st ed. CRC Press, Inc., 1994.
- [3] V.-D. Nguyen, “Constructing force-closure grasps,” in *Proc. of the IEEE Int. Conf. on Robotics and Automation*, vol. 3, 1986, pp. 1368–1373.
- [4] J. Ponce and B. Faverjon, “On computing three-finger force-closure grasps of polygonal objects,” *IEEE Transactions on Robotics and Automation*, vol. 11, no. 6, pp. 868–881, dec 1995.
- [5] J. Ponce, S. Sullivan, A. Sudsang, J.-D. Boissonnat, and J.-P. Merlet, “On computing four-finger equilibrium and force-closure grasps of polyhedral objects,” *International Journal of Robotics Research*, vol. 16, no. 1, pp. 11–35, 1997.
- [6] N. S. Pollard, “Closure and quality equivalence for efficient synthesis of grasps from examples,” *International Journal of Robotics Research*, vol. 23, no. 6, pp. 595–614, 2004.
- [7] M. A. Roa and R. Suárez, “Computation of independent contact regions for grasping 3-d objects,” *IEEE Transactions on Robotics*, vol. 25, pp. 839–850, 2009.
- [8] R. Krug, D. Dimitrov, K. Charusta, and B. Iliev, “On the efficient computation of independent contact regions for force closure grasps,” in *Proc. of the IEEE/RSJ International Conference on Intelligent Robots and Systems*, 2010, pp. 586–591.
- [9] A. Sahbani, S. El-Khoury, and P. Bidaud, “An overview of 3d object grasp synthesis algorithms,” *Robotics and Autonomous Systems*, no. 0, pp. –, 2011.
- [10] N. S. Pollard, “Parallel methods for synthesizing whole-hand grasps from generalized prototypes,” Tech. Rep., 1994.
- [11] D. G. Kirkpatrick, B. Mishra, and C. K. Yap, “Quantitative steinitz’s theorems with applications to multifingered grasping,” in *STOC ’90: Proceedings of the twenty-second annual ACM symposium on Theory of computing*, 1990, pp. 341–351.
- [12] M. Fischer and G. Hirzinger, “Fast planning of precision grasps for 3d objects,” in *Intelligent Robots and Systems, 1997. IROS ’97., Proceedings of the 1997 IEEE/RSJ International Conference on*, vol. 1, sep 1997, pp. 120–126 vol.1.
- [13] S. Goyal, A. Ruina, and J. Papadopoulos, “Planar sliding with dry friction part 1. limit surface and moment function,” *Wear*, vol. 143, no. 2, pp. 307–330, 1991.
- [14] R. D. Howe and M. R. Cutkosky, “Practical Force-Motion Models for Sliding Manipulation,” *The International Journal of Robotics Research*, vol. 15, no. 6, pp. 557–572, Dec. 1996.
- [15] M. Ciocarlie, A. Miller, and P. Allen, “Grasp analysis using deformable fingers,” in *Intelligent Robots and Systems, 2005. (IROS 2005). 2005 IEEE/RSJ International Conference on*, aug. 2005, pp. 4122–4128.
- [16] N. Xydias and I. Kao, “Modeling of contact mechanics with experimental results for soft fingers,” in *Intelligent Robots and Systems, 1998. Proceedings., 1998 IEEE/RSJ International Conference on*, vol. 1, oct 1998, pp. 488–493 vol.1.
- [17] R. Krug, D. Dimitrov, K. Charusta, and B. Iliev, “Prioritized independent contact regions for form closure grasps,” in *Proc. of the IEEE/RSJ Int. Conf. on Intelligent Robots and Systems*, 2011.
- [18] M. de Berg, O. Cheong, M. van Kreveld, and M. Overmars, *Computational Geometry Algorithms and Applications*, 3rd ed. Berlin Heidelberg: Springer-Verlag, 2008.
- [19] C. B. Barber, D. P. Dobkin, and H. Huhdanpaa, “The quickhull algorithm for convex hulls,” *ACM Transactions on Mathematical Software*, vol. 22, no. 4, pp. 469–483, 1996.
- [20] Phasespace optical motion capture systems. [Online]. Available: <http://www.phasespace.com/>